International Journal of Fracture **62**: 355–373, 1993.

R-curve modeling of rate and size effects in quasibrittle fracture

ZDENĚK P. BAŽANT[1] and MILAN JIRÁSEK
Northwestern University, Evanston, Illinois 60208, USA

Received 1 November 1992; accepted 26 April 1993

Abstract. The equivalent linear elastic fracture model based on an *R*-curve (a curve characterizing the variation of the critical energy release rate with the crack propagation length) is generalized to describe both the rate effect and size effect observed in concrete, rock or other quasibrittle materials. It is assumed that the crack propagation velocity depends on the ratio of the stress intensity factor to its critical value based on the *R*-curve and that this dependence has the form of a power function with an exponent much larger than 1. The shape of the *R*-curve is determined as the envelope of the fracture equilibrium curves corresponding to the maximum load values for geometrically similar specimens of different sizes. The creep in the bulk of a concrete specimen must be taken into account, which is done by replacing the elastic constants in the linear elastic fracture mechanics (LEFM) formulas with a linear viscoelastic operator in time (for rocks, which do not creep, this is omitted). The experimental observation that the brittleness of concrete increases as the loading rate decreases (i.e. the response shifts in the size effect plot closer to LEFM) can be approximately described by assuming that stress relaxation causes the effective process zone length in the *R*-curve expression to decrease with a decreasing loading rate. Another power function is used to describe this. Good fits of test data for which the times to peak range from 1 sec to 250000 sec are demonstrated. Furthermore, the theory also describes the recently conducted relaxation tests, as well as the recently observed response to a sudden change of loading rate (both increase and decrease), and particularly the fact that a sufficient rate increase in the post-peak range can produce a load-displacement response of positive slope leading to a second peak.

1. Introduction

The rate of loading as well as the load duration is known to exert a strong influence on the fracture behavior of concrete. Much has been learned in the previous studies of Shah and Chandra [1]; Wittmann and Zaitsev [2]; Hughes and Watson [3]; Mindess [4]; Reinhardt [5]; Wittmann [6]; Darwin and Attiogbe [7]; Reinhardt [8]; Liu et al. [9]; Ross and Kuennen [10] and Harsh et al. [11]; in particular, it has been well established that the strength as well as the fracture energy or fracture toughness increases with increasing rate of loading, roughly as a power function of the loading rate. The previous studies, however, focused mainly on the size effect under dynamic loading, at which the loading rates are very high. At such high rates, the rate effect is mainly due to the thermally activated process of bond ruptures, arising from the effect of stress on the Maxwell-Boltzmann distribution of thermal energies of atoms and molecules.

In this study, we focus on the rate effect at static loading rates at which the creep properties of a material such as concrete begin to play also a significant role, aside from the thermal activation of bond ruptures. The rate effect at such low rates, which is no doubt closely related to the effect of load duration, needs to be known for the design of civil engineering structures carrying high permanent loads or subjected to long time thermal or shrinkage stresses. For such conditions (which are, for example, important for the fracture of dams), the rate effect in concrete

[1] Walter P. Murphy Professor of Civil Engineering.

fracture has been essentially unexplored until the recent experimental studies of Bažant and Gettu [12–15].

The difficulty for materials such as concrete (which also includes rocks and tough ceramics) is that a nonlinear fracture model taking into account the existence of a large fracture process zone is required. Such materials, nowadays widely called quasibrittle, exhibit a transitional size effect in terms of their nominal strength; for small sizes, the behavior is close to plasticity, for which there is no size effect, while for very large sizes the behavior approaches linear elastic fracture mechanics (LEFM), for which the size effect is the strongest possible. As recently discovered (Bažant and Gettu [12–15]), the size effect plot, i.e. the plot of the nominal strength versus the characteristic structure size, is significantly influenced by the loading rate or loading duration. Generally, the loading rate or duration significantly influence the brittleness. Mathematical modeling of this phenomenon is the principal aim of this study.

In previous work, the effect of loading rate on the size effect has been approximately described by quasielastic analysis, in which the behavior at each loading rate for all the specimen sizes is described according to LEFM with an elastic modulus that in effect represents the well-known effective modulus for creep. Such analysis brought to light the changes of brittleness; it, however, cannot be used as a general model if, e.g., the loading rate would vary with time.

In this study, we will attempt a more general and fundamental model, which can be readily generalized to arbitrary loading histories. The model will represent an adaptation of quasilinear elastic fracture analysis by means of the so-called R-curves. The general principles of this approach, without any experimental verification, have already been suggested in Bažant [16, 17]. In the present study we refine and extend this mathematical model and compare it to test data.

The most general and fundamental approach for capturing both the size and rate effects in the fracture of concrete and other quasibrittle materials is of course a constitutive model for the evolution of damage in the fracture process zone, with an appropriate localization limiter. Such a model, which will be required for general finite element codes, should be the objective of future investigations.

2. Basic equations

The R-curve (resistance curve) approach represents an attempt to describe the nonlinearity of the law of crack propagation in quasibrittle materials using an approximately equivalent linear model in which the fracture energy is considered to depend on the length of an equivalent linear elastic crack. This equivalent crack is defined as a crack in a linear elastic material having the same compliance as the actual specimen with a large nonlinear fracture process zone (Fig. 1).

Let us denote the initial crack length by a_0 and the current crack length by a. It is often more convenient to work with nondimensional quantities $\alpha_0 = a_0/d$ and $\alpha = a/d$, where d is the total length of the ligament (Fig. 1). According to LEFM, an applied load P causes a load-point displacement

$$u = \frac{P}{E'b}\bar{C}(\alpha), \tag{1}$$

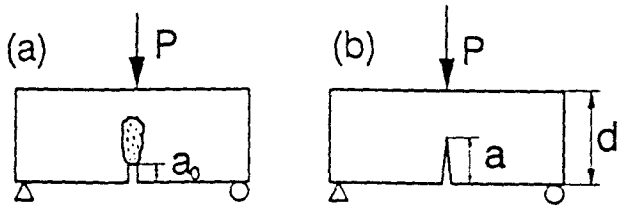

Fig. 1. 3PB specimen with (a) a nonlinear process zone, (b) an equivalent elastic crack.

a crack-mouth opening displacement (CMOD)

$$\Delta = \frac{P}{E'b}\delta(\alpha), \tag{2}$$

and a stress singularity described by the stress intensity factor

$$K = \frac{P}{b\sqrt{d}}k(\alpha), \tag{3}$$

where $E' = E$ for plane stress, $E' = E/(1 - \nu^2)$ for plane strain (E and ν are Young's modulus and Poisson's ratio, respectively), b is thickness of the specimen and $\bar{C}(\alpha)$, $\delta(\alpha)$, $k(\alpha)$ are nondimensional functions depending on geometry. It can be shown (e.g. Bažant and Cedolin [16]) that $\bar{C}(\alpha)$ and $k(\alpha)$ are related by

$$\bar{C}(\alpha) = \bar{C}(0) + 2\int_0^\alpha k^2(\bar{\alpha})\,\mathrm{d}\bar{\alpha}, \tag{4}$$

where $\bar{C}(0)$ is the compliance of the same specimen without any crack. For a three-point-bend (3PB) specimen with span-to-depth ratio $l:d = 2.5:1$ we have (Bažant and Kazemi [19]

$$\bar{C}(0) = \frac{l^3}{4d^3} + \frac{3l(1+\nu)}{5d} = 5.406 + 1.5\nu, \tag{5}$$

$$k(\alpha) = 3.75\sqrt{\pi\alpha}(1-\alpha)^{3/2}(1 - 2.5\alpha + 4.49\alpha^2 - 3.98\alpha^3 + 1.33\alpha^4), \tag{6}$$

$$\delta(\alpha) = 14.1\alpha[0.76 - 2.28\alpha + 3.87\alpha^2 - 2.04\alpha^3 + 0.66(1-\alpha)^{-2}]. \tag{7}$$

The graphs of nondimensional functions $k(\alpha)$ and $\delta(\alpha)$ are shown in Fig. 2a.b.

The Griffith criterion for crack propagation in perfectly brittle materials states that the crack can propagate if the energy needed to create a new free surface is balanced by the elastic energy release from the structure. This condition is equivalent to $K = K_c$, where K is the actual stress intensity factor and K_c its critical value, called fracture toughness.

The usual rate-independent version of the R-curve model for crack propagation in quasi-brittle materials is based on the assumption that the energy needed to propagate the crack is not constant, but increases due to growth of the nonlinear fracture process zone with increasing crack length. According to this assumption, K_c is replaced by the function,

$$K_R(c) = \sqrt{E'R(c)}, \tag{8}$$

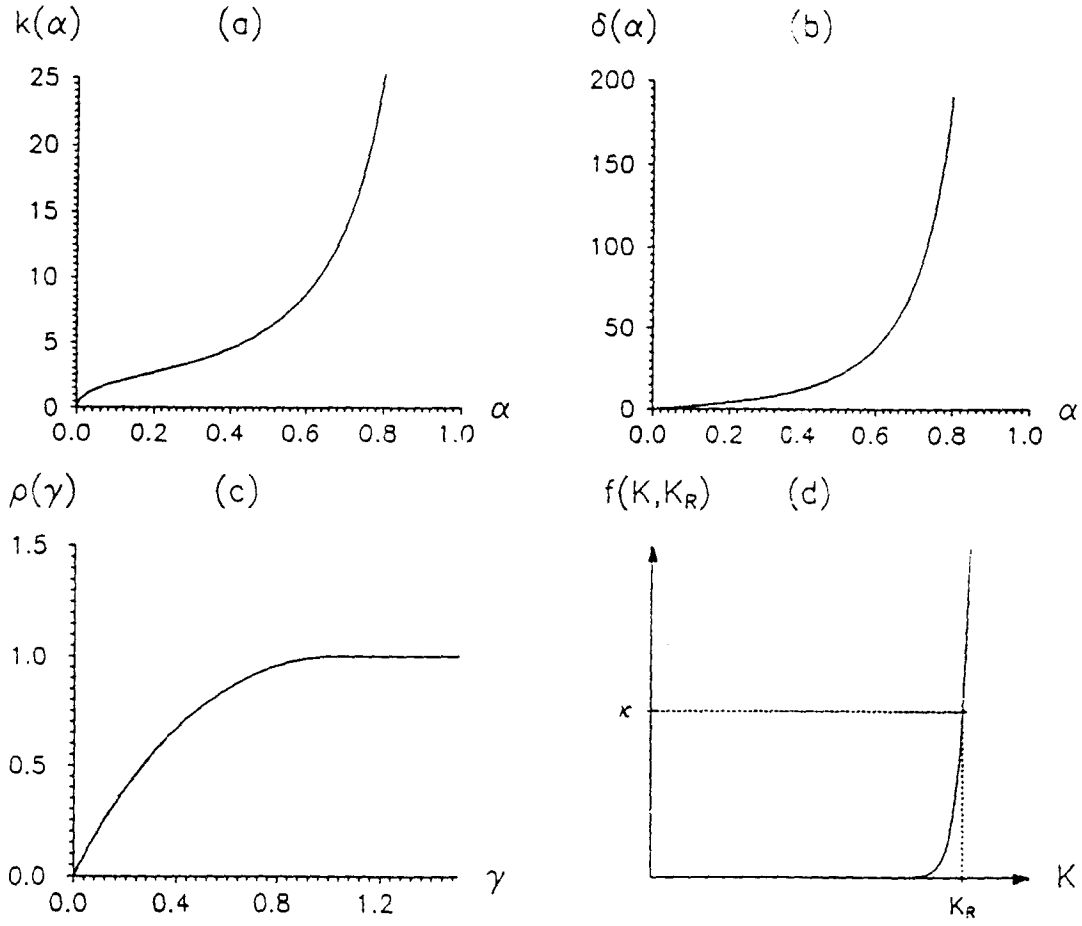

Fig. 2. Graphs of (a) $k(\alpha)$, (b) $\delta(\alpha)$, (c) $\rho(\gamma)$, (d) $f(K, K_R)$

which depends on the crack propagation distance $c = a - a_0$. The resistance function $R(c)$, whose graph is called the R-curve, can be determined solely from maximum loads of similar specimens of different sizes, using the size effect method described in Bažant, Gettu and Kazemi [20]. Aside from geometry, $R(c)$ depends on two material constants G_f and c_f representing the fracture energy and the fracture process zone length at the peak load for an infinitely large specimen. Based on the size effect law (see [18], Sec. 12.3 and 13.9), it has been shown (Bažant and Kazemi [19, 20]) that the shape of the R-curve is determined by the equations

$$\frac{R}{G_f} = \frac{c}{c_f}\frac{g'(\alpha)}{g'(\alpha_0)}, \tag{9}$$

and

$$\frac{c}{c_f} = \left[\frac{g(\alpha)}{g'(\alpha)} - \alpha + \alpha_0\right]\frac{g'(\alpha_0)}{g(\alpha_0)}, \tag{10}$$

where $g(\alpha) = k^2(\alpha)$ = nondimensional function depending only on geometry. Choosing a sequence of α-values, one calculates for each of them the value of c/c_f and the corresponding R/G_f.

Obviously, the relation between R/G_f and c/c_f depends only on the shape (geometry) of the structure. It is therefore convenient to separate the effects of geometry from the material properties and write

$$R(c) = G_f \rho(\gamma), \quad \gamma = \frac{c}{c_f}, \tag{11}$$

where ρ is the normalized resistance function depending on geometry only. Its graph (the normalized R-curve) for a three-point bend (3PB) specimen with span-to-depth ratio 2.5:1 is shown in Fig. 2c.

Combining (8) and (11), we get

$$K_R(c) = \sqrt{E' G_f}\sqrt{\rho(\gamma)} = K_f\sqrt{\rho(\gamma)}, \tag{12}$$

where K_f is the fracture toughness for an infinitely large specimen.

To capture the effects of the loading rate, we assume that the crack propagation rate $\dot{a} = da/dt$ depends on the current values of K and K_R:

$$\dot{a} = f(K, K_R). \tag{13}$$

Since $K = \sqrt{E'G(a)}$, $K_R = \sqrt{E'R(c)}$, this is equivalent to assuming that $\dot{a}$ is a function of $G(a)$ and $R(c)$ where $G(a)$ is the energy release rate. It is clear that $\dot{a}$ should increase with increasing K and with decreasing K_R. But what should be the actual form of the crack growth rate function $f(K, K_R)$? Experimental evidence indicates that changing the loading rate by several orders of magnitude causes the peak loads to change only by a factor less than 2 [14, 15, 26]. Therefore, the crack growth rate function should allow for a very large variation of $\dot{a}$ with only moderate changes of its arguments. This can be achieved by setting

$$f(K, K_R) = \kappa\left(\frac{K}{K_R}\right)^n, \tag{14}$$

where κ and n are constants. It is expected that $n \gg 1$, so that $\dot{a}$ varies with K as indicated in Fig. 2d.

Equations (1) and (2) have been based on the assumption of linear elasticity. Under loading rates spanning over several orders of magnitude, creep effects can play an important role. Creep in the bulk of the specimen can be taken into account by replacing $1/E'$ by an appropriate compliance operator, which yields

$$u(t) = \frac{1}{b}\int_{t_0}^{t} J(t, t')\, \mathrm{d}[P(t')\bar{C}(t')], \tag{15}$$

$$\Delta(t) = \frac{1}{b}\int_{t_0}^{t} J(t, t')\, \mathrm{d}[P(t')\delta(t')]. \tag{16}$$

$J(t,t')$ is the compliance function, which must be determined in advance by measuring or estimating the creep properties of the material. The geometric compliances $\bar{C}$, $\bar{\delta}$ are time dependent because they vary with the relative crack length α, which increases as the crack propagates.

Experiments performed under load control become unstable after the peak load has been reached. To study the descending part of the load-displacement curve, displacement control must be adopted. The available experiments [14, 15, 21] have been performed under a constant CMOD rate. In such a case, the time history of CMOD is described by a linear function

$$\Delta(t) = r(t - t_0), \tag{17}$$

where t_0 is the time at the beginning of the experiment and constant r is the prescribed CMOD rate. The unknown functions $P(t)$ and $\alpha(t)$ describing the variation of the applied load and evolution of the crack length can be determined by solving the crack propagation equation (13) along with (16). Using relations (3), (12), (17) and $a = \alpha d$, we can rewrite the basic equations as

$$\dot{\alpha}(t) = \frac{1}{d} f\left(\frac{P(t)}{b\sqrt{d}} k[\alpha(t)],\ K_f \sqrt{\rho\left[(\alpha(t) - \alpha_0)\frac{d}{c_f}\right]}\right), \tag{18}$$

$$b\Delta(t) = \int_{t_0}^{t} J(t, t')\, \mathrm{d}[P(t')\delta(t')], \tag{19}$$

where the function f is defined by (14). The CMOD history $\Delta(t)$ is specified as input, to simulate the present tests. Alternatively, the load point deflection history $u(t)$ can be specified as input. As still another alternative, the load history $P(t)$ may be specified as input and then, first, (18) is solved for $\alpha(t)$ and, second, $\Delta(t)$ is evaluated from (19). The initial conditions are

$$\alpha(t_0) = \alpha_0, \quad P(t_0) = 0, \quad \Delta(t_0) = 0. \tag{20}$$

3. Numerical solution

To solve the problem numerically, we divide time into equal intervals $\langle t_i, t_{i+1}\rangle$, $i = 0, 1, 2, \ldots, N$, with $t_i = t_0 + i\Delta t$. Suppose that we have already computed approximate values $\alpha_i = \alpha(t_i)$, $P_i = P(t_i)$ for $i = 0, 1, 2, \ldots, j$ and we want to proceed to α_{j+1}, P_{j+1}. Equations (18), (19) can be discretized in $\langle t_j, t_{j+1}\rangle$ as follows:

$$\frac{\alpha_{j+1} - \alpha_j}{\Delta t} = \frac{1}{d} f\left[\frac{P_{j+1} + P_j}{2b\sqrt{d}} k\left(\frac{\alpha_{j+1} + \alpha_j}{2}\right),\ K_f \sqrt{\rho\left[\left(\frac{\alpha_{j+1} + \alpha_j}{2} - \alpha_0\right)\frac{d}{c_f}\right]}\right], \tag{21}$$

$$b\Delta_{j+1} = \sum_{i=0}^{j} J\left(t_{j+1}, \frac{t_{i+1} + t_i}{2}\right)[P_{i+1}\delta(\alpha_{i+1}) - P_i\delta(\alpha_i)]. \tag{22}$$

where $\Delta_{j+1} = \Delta(t_{j+1}) = r(j+1)\Delta t$ for tests with a constant CMOD rate. For convenience let us denote

$$J_{j,i} = J\left(t_{j+1}, \frac{t_{i+1} + t_i}{2}\right), \tag{23}$$

$$\delta_i = \delta(\alpha_i), \tag{24}$$

$$S_{j+1} = \sum_{i=0}^{j-1} J_{j,i}(P_{i+1}\delta_{i+1} - P_i\delta_i). \tag{25}$$

Equations (21), (22) are two nonlinear equations for unknowns P_{j+1}, α_{j+1}. Noting that (22) is linear with respect to P_{j+1}, we can express P_{j+1} as

$$P_{j+1} = \left[\frac{b\Delta_{j+1} - S_{j+1}}{J_{j,j}} + P_i\delta_j\right]\frac{1}{\delta(\alpha_{j+1})}, \tag{26}$$

and substitute this expression into (21). We end up with a nonlinear equation with only one unknown α_{j+1}. As the right-hand side of (21) is highly nonlinear, a robust numerical procedure must be chosen to assure convergence. After some experimentation, an algorithm based on a secant rather than tangent formula has been adopted.

Special treatment is necessary in the first few time steps when the process zone is very small and K_R is therefore close to zero. In fact, at time t_0 we have $K_R = 0$, $K = 0$ and the ratio K/K_R is not defined. Even though we do not need to evaluate this ratio at t_0 but only at $t_0 + (\Delta t/2)$, α is at the beginning of crack propagation very close to α_0 and numerical problems arise due to strong sensitivity of the high power $(K/K_R)^n$ to even very small changes of α.

To overcome these difficulties, we need to make use of an approximate analytical solution, which can be derived under the simplifying assumptions that $\alpha - \alpha_0 \ll 1$ and that P is a linear function of time

$$P(t) = \bar{P}(t - t_0), \tag{27}$$

where $\bar{P}$ is a constant to be determined later. For small values of $\alpha - \alpha_0$, $k(\alpha)$ can be replaced by $k_0 = k(\alpha_0)$ and $\rho[(\alpha - \alpha_0)d/c_f]$ by $\bar{\rho}(\alpha - \alpha_0)d/c_f$, where $\bar{\rho} = \rho'(0)$. Equation (14) can now be transformed to

$$\dot{\alpha} = \frac{\kappa}{d}\left(\frac{K}{K_R}\right)^n = C_0\left(\frac{t - t_0}{\sqrt{\alpha - \alpha_0}}\right)^n, \tag{28}$$

where

$$C_0 = \frac{\kappa}{d}\left(\frac{\bar{P}k_0\sqrt{c_f}}{bdK_f\sqrt{\bar{\rho}}}\right)^n. \tag{29}$$

Solving the approximate crack propagation equation (28) by separation of variables, we get

$$\alpha = \alpha_0 + C_1(t - t_0)^{(2n+2)/(n+2)}, \tag{30}$$

where

$$C_1 = \left(C_0 \frac{n+2}{2n+2}\right)^{2/(n+2)} \tag{31}$$

It is interesting to note that if n is large, $\alpha - \alpha_0$ is approximately proportional to $(t - t_0)^2$.

Except for $\bar{P}$, all the quantities in expressions (29) and (31) defining C_1 are known. $\bar{P}$ can be determined from the load-CMOD relation (16). If $\alpha - \alpha_0 \ll 1$, we can treat $\delta(\alpha(t))$ as approximately equal to $\delta_0 = \delta(\alpha_0)$. Using $P = \bar{P}(t - t_0)$ and $\Delta = r(t - t_0)$, (16) can be simplified to $br(t - t_0) = \bar{P}\delta_0 \int_{t_0}^{t} J(t, t')\,dt'$, from which

$$\bar{P} = \frac{br(t - t_0)}{\delta_0 \int_{t_0}^{t} J(t, t')\,dt'}. \tag{32}$$

The fact that the right-hand side of (32) depends on time contradicts the assumption $\bar{P} = \text{const.}$, but we can think of each time instant $t = t_i$ separately, approximating the history of $P(t)$ in the interval $\langle t_0, t_i \rangle$ by a linear function whose slope depends on the time instant under consideration. The analytical solution (30) is used only in the first few steps. We exploit it to initialize the crack propagation and get a reasonable estimate for the initial crack propagation rate. In fact we need only an order-of-magnitude estimate as the initial approximation for the previously described numerical procedure. The rates of crack propagation at the very beginning have nearly no influence on the later stages of the process and they are needed only as the approximations to start with. Therefore, the present simplifications are justified.

It has been observed experimentally [20] that after the peak load $R(c)$ ceases increasing but remains constant. The explanation is that after the peak load the process zone length ceases growing and travels across the ligament approximately as a rigid body.

4. Comparison of theory to constant CMOD rate tests

Performance of the proposed model has been compared with the experimental results reported [14], [15], [21] and [26].

Bažant and Gettu investigated simultaneous rate and size effect for three-point-bend concrete specimens. Each experiment was performed under a constant CMOD rate. They tested specimens of three different sizes (d = 38 mm, 76 mm, 152 mm) and applied the CMOD rates ranging from 4×10^{-11} m/s to 10^{-5} m/s, with the corresponding times to peak ranging from 3 days to 1 second. Table 1 shows the peak loads recorded for each test. Most of the specimen were tested at 28 days after casting, but some of them were much older (up to 120 days). To get comparable data, the measured peak loads have been adjusted to the same age (28 days) using a

Table 1. Experimental results by Bažant and Gettu [14]

Depth [mm]	CMOD rate [m s]	Age [days]	Peak load [N]
38	$1.1\,10^{-5}$	28	2217
38	$1.1\,10^{-5}$	28	1883
38	$8.4\,10^{-6}$	28	1794
38	$2.4\,10^{-8}$	28	1639
38	$1.8\,10^{-8}$	28	1774
38	$1.8\,10^{-8}$	28	1818
38	$7.1\,10^{-10}$	40	2256
38	$7.1\,10^{-10}$	38	1891
38	$7.1\,10^{-10}$	39	2128
38	$3.8\,10^{-11}$	120	2007
76	$1.4\,10^{-5}$	28	3612
76	$1.4\,10^{-5}$	28	3946
76	$1.4\,10^{-5}$	28	3014
76	$5.3\,10^{-8}$	28	3059
76	$4.3\,10^{-8}$	28	2750
76	$3.6\,10^{-8}$	28	2790
76	$1.1\,10^{-9}$	30	3153
76	$1.0\,10^{-9}$	46	3465
76	$9.4\,10^{-10}$	42	3417
76	$7.4\,10^{-11}$	108	2995
152	$2.1\,10^{-5}$	28	6158
152	$2.1\,10^{-5}$	28	5919
152	$2.1\,10^{-5}$	28	5406
152	$7.1\,10^{-8}$	28	5007
152	$7.1\,10^{-8}$	28	4210
152	$7.1\,10^{-8}$	28	4185
152	$1.7\,10^{-9}$	31	5239
152	$1.4\,10^{-9}$	32	4216
152	$1.4\,10^{-9}$	38	4085
152	$1.3\,10^{-10}$	90	4332

simple approximate empirical formula

$$P_{\text{peak},28} = P_{\text{peak},t_0}\sqrt{0.86 + \frac{4}{t_0}}, \tag{33}$$

where t_0 is the age at testing in days, P_{peak,t_0} is the measured peak load and $P_{\text{peak},28}$ is the corrected peak load. The creep compliance function $J(t, t')$ has been approximated by the well-known double-power law (see [18], Sec. 9.4):

$$J(t, t') = \frac{1}{E_0}[1 + \phi_1(t'^{-m} + \alpha)(t - t')^n]. \tag{34}$$

In agreement with the data from [14], the parameters of this law were set as follows: $E_0 = 48.4\,\text{GPa}$, $\phi_1 = 3.93$, $m = 0.306$, $n = 0.133$, $\alpha = 0.00325$.

It is clear from Table 1 and Fig. 3a that the experimentally determined values of the peak load suffer from considerable scatter, which can be explained by the fact that the specimens

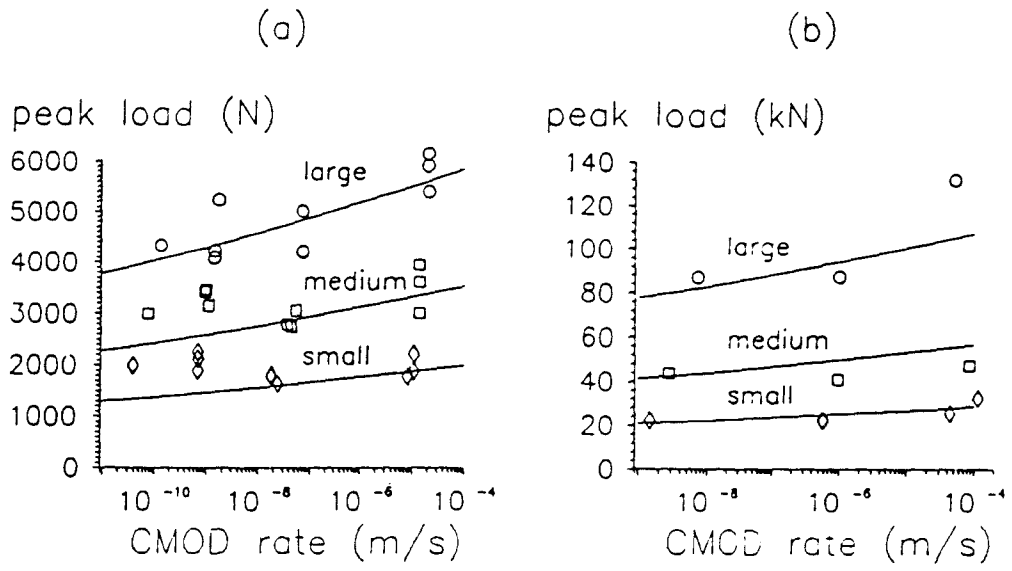

Fig. 3. Comparison with experiments for concrete: (a) three point bending, (b) wedge splitting.

were cast from several batches of concrete. Nevertheless, some general trends can still be observed:

- The peak loads increase with increasing rate of loading.
- The rate dependence of peak loads is stronger for large specimens than for small ones.
- The nominal strength decreases with increasing size, approximately following the size effect law proposed by Bažant [24].
- The size effect on peak loads is stronger for slow loading rates than for fast ones.

It may be somewhat surprising that the size effect and the rate effect in concrete appear to be mutually dependent. In terms of size effect, a decreasing rate of loading causes a shift towards more brittle behaviour. The same phenomenon can be described in terms of rate effect as an increase of rate sensitivity with increasing size.

In contrast to concrete, no interaction of size and rate effect could be observed for limestone [15]. This could probably be explained by absence of creep in limestone, both within the bulk of the specimen and within the fracture process zone. This means that the rate effect in limestone is due solely to the thermally activated process of bond ruptures, producing the crack surfaces.

In an attempt to fit the aforementioned experimental data by the proposed rate-dependent R-curve model, it has been discovered that the originally proposed version does not exhibit any shift of brittleness. It was therefore not difficult to get a reasonable agreement between theory and experiments for limestone (Fig. 4), while for concrete (Fig. 3a) it was impossible to get a good agreement for all the rates and all the sizes at the same time.

It is nevertheless encouraging that the model can capture both the size effect and the rate effect, although not their mutual interaction. Let us briefly describe the role of free parameters, whose values can be adjusted to get the best fit of experimental data:

- Parameters κ and K_f are mutually dependent, so that only one of them can be regarded as a free parameter. By increasing K_f or decreasing κ, the peak loads are increased for all the rates and sizes in the same ratio.

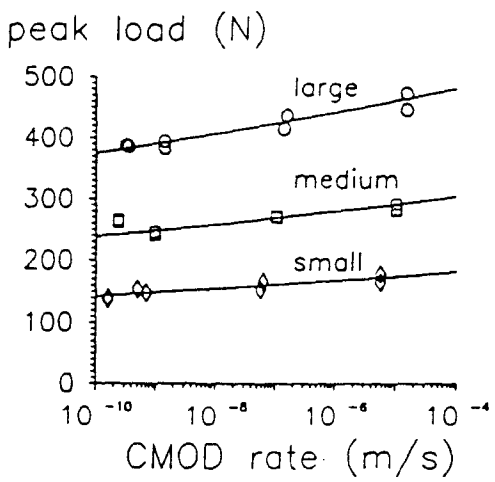

Fig. 4. Comparison with experiments for limestone.

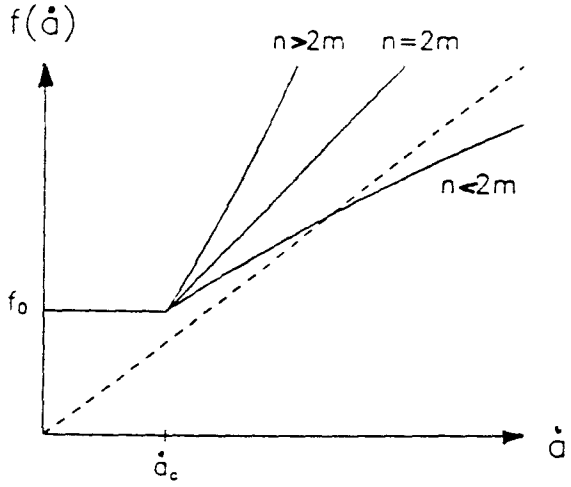

Fig. 5. Graph of f for different ratios n $2m$.

- Parameter n affects mainly the rate sensitivity (for all the sizes in the same manner). By increasing n, one can decrease the slope of the rate effect curve, which is indicated by experiments to be roughly linear when the CMOD rate is plotted in a logarithmic scale.
- Parameter c_f affects brittleness, and does so for all the rates in roughly the same manner. Increasing c_f causes a shift toward the left on the size effect curve, i.e. to a more ductile behaviour.

To decrease the rate sensitivity of the model to realistic values, a very large exponent n is needed. For example to fit the data on 3PB experiments on concrete [14], n had to be set equal to 38 (Fig. 3a), and for similar experiments on limestone [15] even to 55 (Fig. 4)!

The rate dependent R-curve model has also been used to model wedge-splitting tests on concrete reported in [21]. Due to considerable scatter in these large-scale tests, it is impossible to make any quantitative conclusions. However, similar trends as in 3PB tests can be observed (Fig. 3b). The value of the exponent n came out to be 35, which is about the same as for the aforementioned 3PB experiments.

5. A generalization: rate-dependent process zone length

The original version of the rate-dependent R-curve model presented in the foregoing suffers by a serious drawback: It is not capable of modeling the rate-dependent shift of brittleness observed experimentally by Bažant and Gettu [14]. In an attempt to increase flexibility of our model, we may replace the constant value of c_f (process zone length at peak load for an infinitely large specimen) by a rate-dependent function $c_f(\dot{a})$. The rate-dependence of c_f is not illogical. Stress relaxation in the fracture process zone may be expected to cause the stress profile along the crack extension line to develop a steeper drop to zero, spanning a shorter length, which means that the effective fracture process zone length should be smaller at slower crack propagation.

As explained in Section 3, c_f is the basic parameter affecting brittleness. Because brittleness is seen to decrease with increasing rate, c_f should be an increasing function of $\dot{a}$. However, c_f should vary only by a factor of 10 while the rate of loading (and therefore also the rate of crack

propagation) varies over five orders of magnitude. It is therefore reasonable to use a power function with a low exponent

$$c_f = c_{f0}\left(\frac{\dot{a}}{\dot{a}_0}\right)^{1/m}, \tag{35}$$

where $m \gg 1$. For the sake of dimensionality we have introduced here, in addition to m, two more parameters $c_{f0}, \dot{a}_0$, but only one of them is independent. The other one can be preset to any (positive) fixed value without any loss of generality.

With c_f dependent on $\dot{a}$, the crack propagation equation (13) now becomes an implicit law for the crack propagation rate $\dot{a}$. If the model is to be physically reasonable, there must exist a unique nonnegative solution $\dot{a}$ for any possible situation. This condition imposes a serious restriction on the value of m. A simple analysis of this restriction can be performed if we approximate $\rho(c/c_f)$ by a piecewise linear function

$$\rho\left(\frac{c}{c_f}\right) = \frac{c}{c_f} \quad \text{if } \frac{c}{c_f} < 1, \qquad \rho\left(\frac{c}{c_f}\right) = 1 \quad \text{if } \frac{c}{c_f} \geqslant 1. \tag{36}$$

The function f defined by (14) can now be written as

$$f(K, K_R) = \kappa\left(\frac{Pk}{b\sqrt{d}K_f}\right)^n \left[\rho\left(\frac{c}{c_f(\dot{a})}\right)\right]^{-n/2} = f_0\left[\rho\left(\frac{c}{c_f(\dot{a})}\right)\right]^{-n/2}. \tag{37}$$

Suppose that the current values of P, k, c are given and we want to solve (14) for unknown $\dot{a}$. Denote by $\dot{a}_c$ the value of $\dot{a}$ for which $c_f(\dot{a}) = c$. If $0 < \dot{a} < \dot{a}_c$, then $c_f(\dot{a}) < c$, $\rho(c/c_f(\dot{a})) = 1$ and $f(K, K_R) = f_0$. If $\dot{a} > \dot{a}_c$, then $c_f(\dot{a}) > c$, $\rho(c/c_f(\dot{a})) = c/c_f(\dot{a})$ and

$$f(K, K_R) = f_0\left[\frac{c}{c_{f0}(\dot{a}/\dot{a}_0)^{1/m}}\right]^{-n/2} = f_0\left(\frac{\dot{a}}{\dot{a}_c}\right)^{n/2m}. \tag{38}$$

The right hand side of (38) is graphically presented in Fig. 5 for three different cases. It is clear that if $n/2m < 1$, equation $\dot{a} = f(K, K_R)$ has a unique positive solution for any values of f_0 and $\dot{a}_c$. However, if $n/2m > 1$, the equation has no solution or two solutions depending on whether $f_0 > \dot{a}_c$ or $f_0 < \dot{a}_c$. Thus, to ensure a proper formulation of the crack propagation equation, the parameter m in (35) must be larger than $n/2$, n being the exponent in (14). This condition has been derived under the simplifying assumption (36), but numerical calculations reveal that the method indeed does not converge if $m < n/2$ and sometimes even if m is only slightly above $n/2$.

It has been mentioned in Section 4 that, in order to ensure realistic rate sensitivity, n must assume very large values, typically between 30 and 40. On the other hand, m should not be too large if we want to get a substantial shift of brittleness. Unfortunately, $m > n/2$ must hold, otherwise the problem of crack propagation is not well-posed. The best fit of experimental results that could be constructed with rate-dependent c_f is still underestimating the measured peak

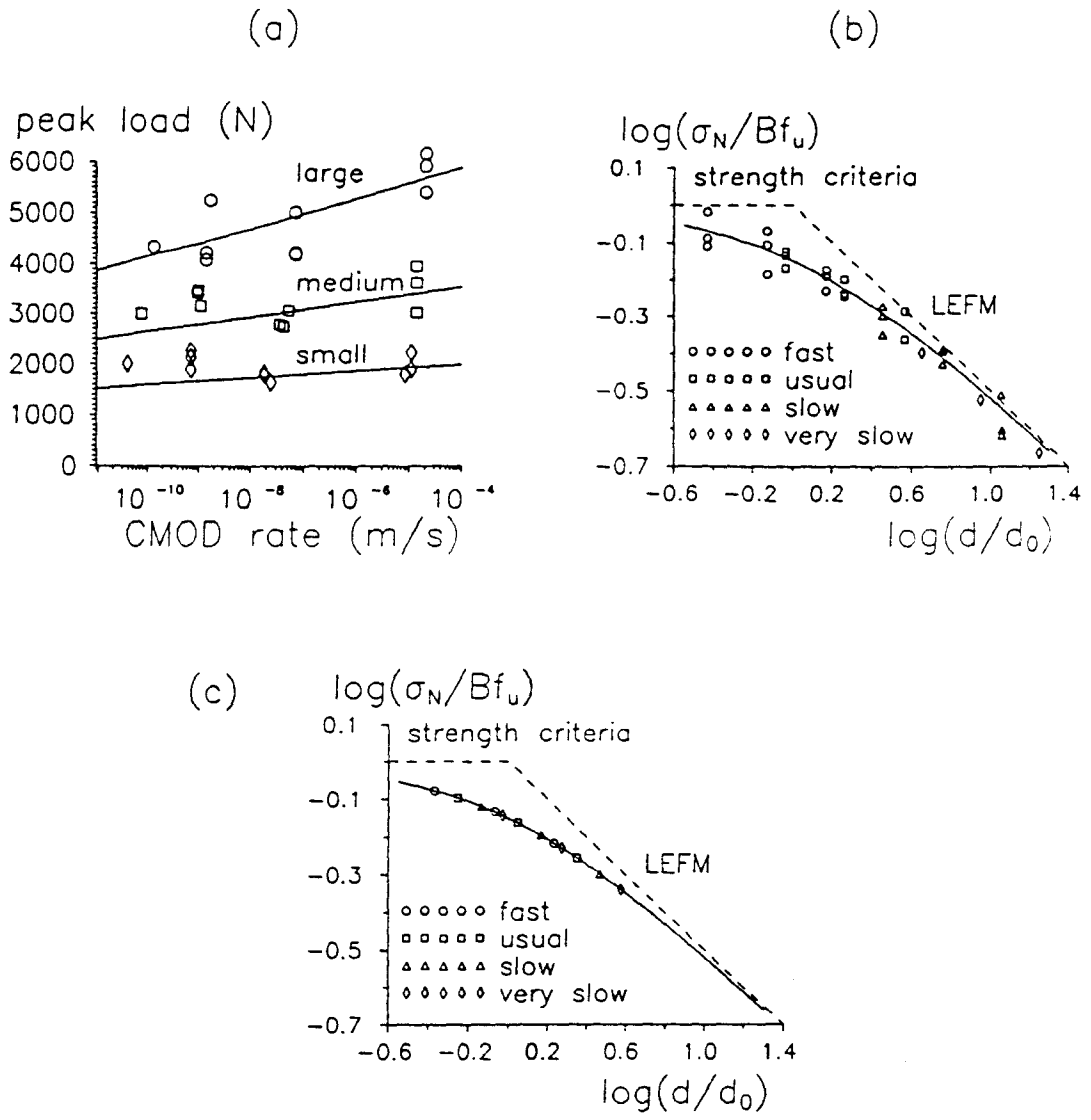

Fig. 6. Generalized model with variable c_f: (a) rate effect, (b) experimental size effect, (c) numerical size effect.

loads for small specimens under slow loading rates (Fig. 6a). In terms of the size effect, this means that the parameter d_0 in the size effect law [24]

$$\sigma_N = \frac{Bf_t}{\sqrt{1 + \dfrac{d}{d_0}}} \tag{39}$$

does not change with rate as much as it should, according to the tests of concrete (see Fig. 6b, c).

The theoretical curves in Fig. 6a correspond to the following set of parameters: $\kappa = 8 \times 10^{-6}$ m s, $K_f = 9 \times 10^5$ Nm$^{-3/2}$, $n = 29$, $c_{f0} = 0.014$ m, $\dot{a}_0 = 0.01$ m/s, $m = 17$. Let us emphasize again that only four of these six parameters are independent.

6. Comparison to tests with a sudden rate change

Another set of experiments on rate effect in concrete fracture was performed by Bažant, Gu and Faber [25], who studied the effect of a sudden change of loading rate. In their tests on 3PB notched specimens, the initial CMOD rate was held constant in the prepeak range and in a part of the post-peak range. After the load decreased from its peak value P_1 to some lower value P_c, the CMOD rate was suddenly increased or decreased by several orders of magnitude and the test continued with the new value of a constant CMOD rate. This resulted into a sudden change of slope in the load-CMOD diagram. For a sufficiently large increase of the loading rate, the load started increasing again and a second peak P_2 could be observed (Fig. 7a). On the other hand, a decrease of the loading rate was followed by a fast drop of the load-CMOD curve (Fig. 7b). The rate-dependent R-curve model exhibits qualitatively the same behavior (Fig. 7c). The tests suggest that, after a rate change, the curve for the new rate asymptotically approaches the curve for a constant rate test with a rate equal to the new rate. The theory agrees with this behavior also (Fig. 7c).

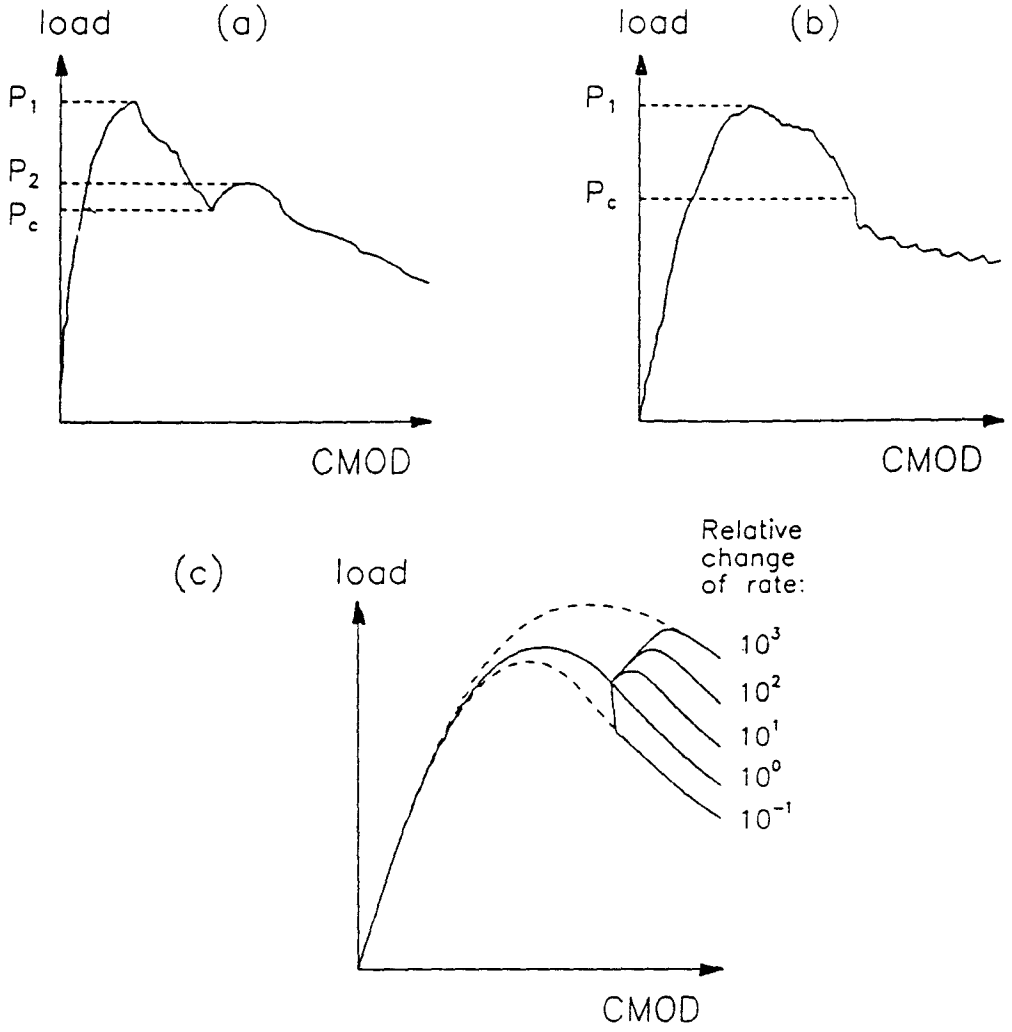

Fig. 7. Load-CMOD curves: (a) experimental curve (rate increased), (b) experimental curve (rate decreased), (c) theoretical curves.

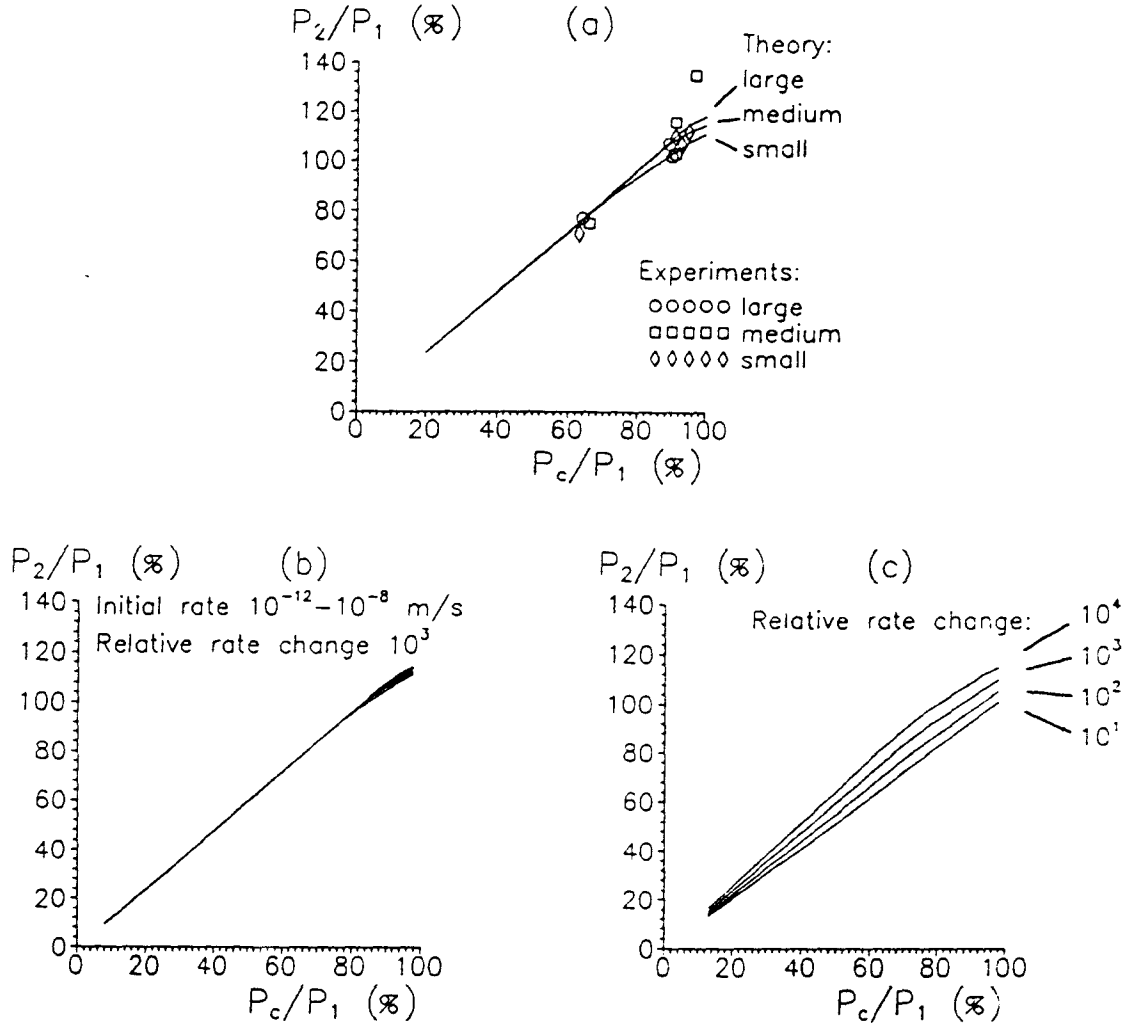

Fig. 8. Second peak versus load at rate change: (a) effect of size, (b) effect of initial rate, (c) effect of relative rate change.

Quantitative agreement between theory and experiments can be verified by plotting the ratio P_2/P_1 versus P_c/P_1 for all available results. The points marked by different symbols in Fig. 8a correspond to tests on specimens with three sizes (d = 38 mm, 76 mm, 152 mm) in which the rate increased by three orders of magnitude (on the average from 10^{-8} m s to 10^{-5} m s). The results seem to be independent of size.

The relationship between the two nondimensional ratios P_c/P_1 and P_2/P_1 can be calculated using the rate-dependent R-curve model described in previous sections. Instead of trying to adjust the parameters so as to fit the experimental data, their values were taken from the best fit of tests by Bažant and Gettu [14] constructed in Section 5. It is gratifying that these parameter values lead to a satisfactory agreement with measurements by Bažant, Gu and Faber [25].

The theoretical curves are only slightly dependent on size (Fig. 8a) and almost independent of the initial rate (for the same relative rate change—Fig. 8b). But, as expected, they are sensitive to the relative rate change (Fig. 8c).

7. Comparison to relaxation tests

The paper by Bažant and Gettu [14] reported still another type of experiment on the rate effect in concrete fracture – relaxation tests. The CMOD rate was initially held constant and after some time (usually in the post-peak range) suddenly decreased to zero. This type of test can be

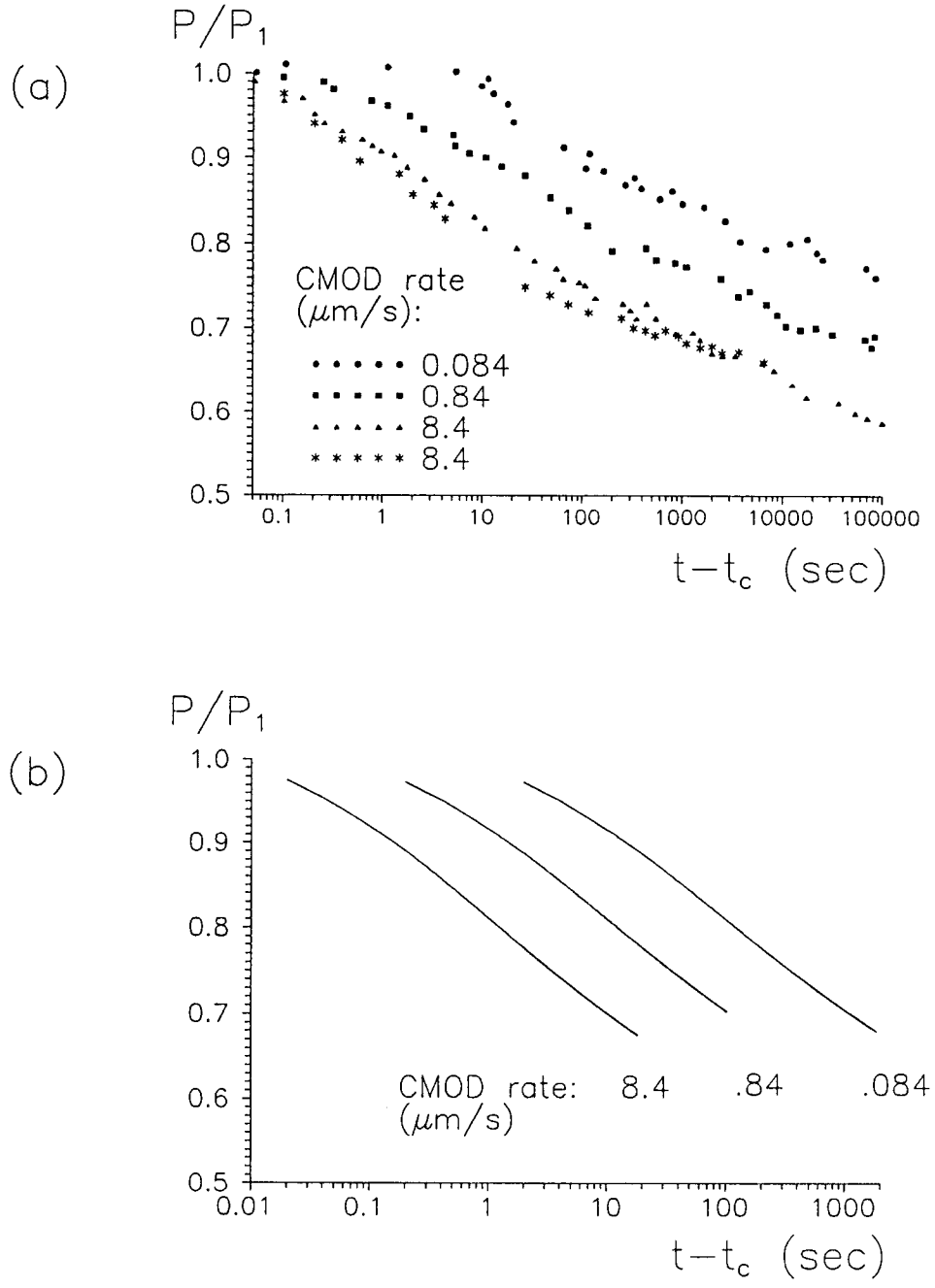

Fig. 9. Relaxation curves for different initial rates: (a) experimental, (b) theoretical.

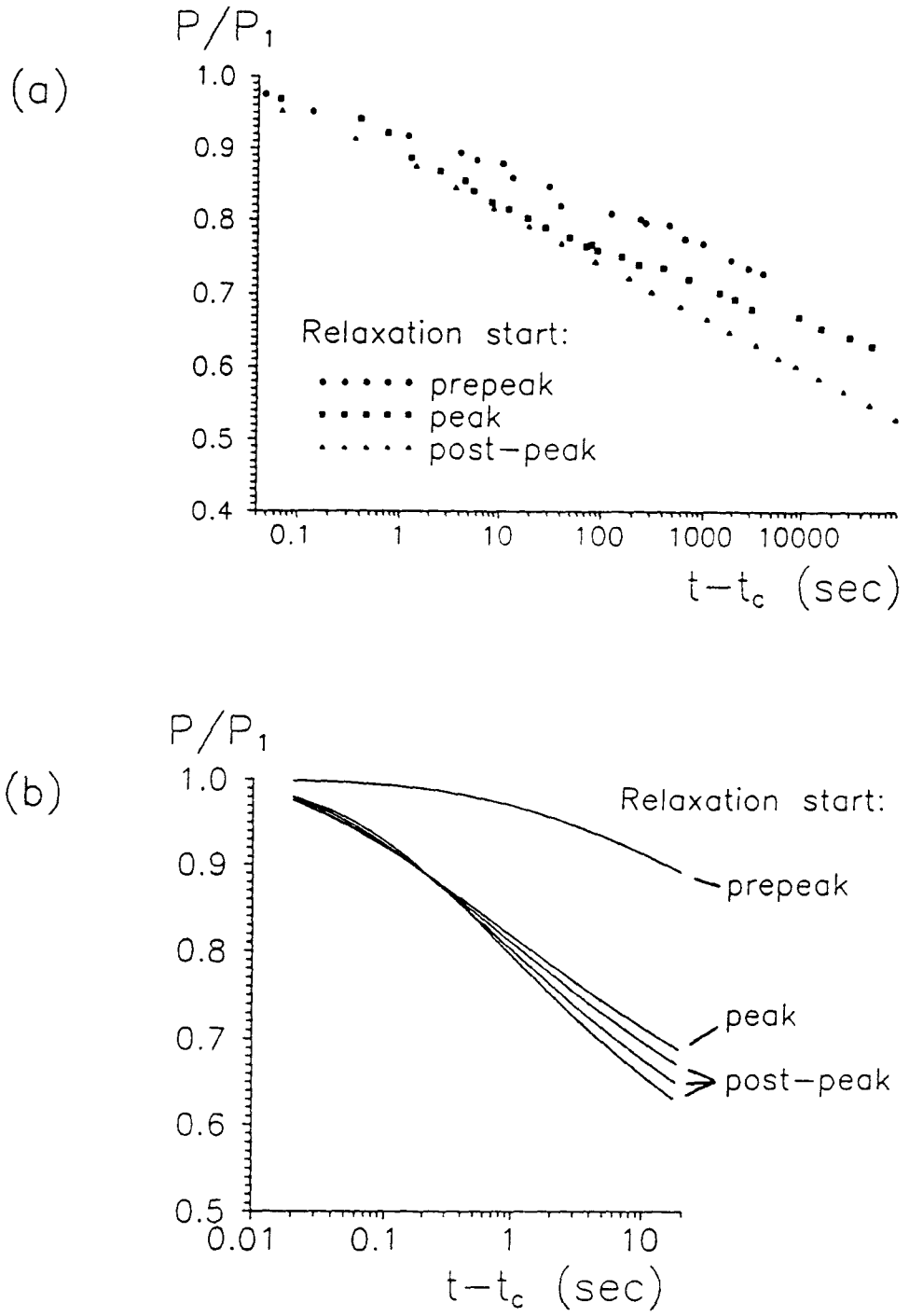

Fig. 10. Relaxation curves for different loads at relaxation start: (a) experimental, (b) theoretical.

regarded as a limit case of the experiments with a sudden change of rate. All tests were performed on medium size 3PB specimens ($d = 76$ mm).

In the first series of experiments, the initial rates were different and relaxation started in the post-peak range at about 85 percent of the peak load. Denoting the time at which relaxation started by t_c and the corresponding load by P_c, one can plot the relaxation curves $P(t)/P_c$ versus $t - t_c$. The experimental and theoretical relaxation curves are shown in Fig. 9. A qualitative

agreement can be observed – the curves corresponding to different initial rates have the same final slope in a logarithmic plot and are shifted with respect to each other. However, the slope of the theoretical curves is much steeper than of the experimental ones.

The second series of experiments was conducted with the same initial rate ($r = 8.5 \times 10^{-6}$ m s) but relaxation started at different stages – in the prepeak range, at peak, and at different load levels in the post-peak range. Figure 10c reveals again only a qualitative agreement – the relaxation curves starting in the post-peak range lie below the curve starting approximately at peak, which in turn lies below the curve starting in the pre-peak range. The theoretical curves are again steeper than the experimental ones.

8. Conclusions

1. The equivalent linear elastic fracture model based on an R-curve (a curve characterizing the variation of critical energy release rate with crack propagation length) can be generalized to the rate effect if the crack propagation velocity is assumed to depend either on the ratio of the stress intensity factor to its critical value based on the R-curve, or on the difference between these two variables. This dependence may be assumed in the form of an increasing power function with a large exponent.
2. The creep in the bulk of a concrete specimen must also be taken into account, which can be done by replacing the elastic constants in the LEFM formulas with a linear viscoelastic operator in time. For rocks, which do not creep, this is not necessary.
3. The experimental observation that the brittleness of concrete increases with a decreasing loading rate (i.e. the response shifts in the size effect plot closer to linear elastic fracture mechanics) can be at least approximately modeled by assuming the effective fracture process zone length in the R-curve expression to decrease with a decreasing rate. This dependence may again be described by a power function.
4. Good agreement with the previous test results for concrete and limestone, recently measured at very different loading rates, with times to peak ranging from 1 second to 250000 seconds, is achieved.
5. The model can also predict the following phenomena recently observed in the laboratory:
   (a) When the loading rate is suddenly increased, the slope of the load-displacement diagram suddenly increases. For a sufficient rate increase, the slope becomes positive even in the post-peak range, and later in the test a second peak, lower or higher than the first peak, is observed.
   (b) When the rate suddenly decreases, the slope suddenly decreases and the response approaches the load-displacement curve for the lower rate.
   (c) When the displacement is arrested, relaxation causes a drop of load, approximately following a logarithmic time curve.

Acknowledgment

Financial support under NSF Grant No. MSS-9114476 to Northwestern University is gratefully acknowledged. Partial support for the experiments has been obtained from the Center for Advanced Cement-Based Materials at Northwestern University.

References

1. S.P. Shah and S. Chandra, *American Concrete Institute, Journal* 67 (1970) 816–825.
2. F.H. Wittmann and Y. Zaitsev, in *Mechanical Behavior of Materials, Proceedings, 1971 International Conference Society of Material Science*, Japan (1972) 84–95.
3. B.P. Hughes and A.J. Watson, *Magazine of Concrete Research* 30 (1978) 189–199.
4. S. Mindess, in *Application of Fracture Mechanics to Cementitious Composites*, S.P. Shah (ed.), Martinus Nijhoff Publishers, Dordrecht (1985) 617–638.
5. H.W. Reinhardt, in *Application of Fracture Mechanics to Cementitious Composites*, S.P. Shah (ed.), Martinus Nijhoff Publishers, Dordrecht (1985) 559–592.
6. F.H. Wittmann, in *Application of Fracture Mechanics to Cementitious Composites*, S.P. Shah (ed.), Martinus Nijhoff Publishers, Dordrecht (1985) 559–592.
7. D. Darwin and E.K. Attiogbe, in *Cement Based Composites: Strain Rate Effects on Fracture*, Mindess and Shah (eds.) (1986) 167–180.
8. H.W. Reinhardt, *Cement Based Composites: Strain Rate Effects on Fracture*, S. Mindess and S.P. Shah (eds.) (1986) 1–14.
9. Z.-G. Liu, S.E. Swartz, K.K. Hu and Y.-C. Kan, *Fracture of Concrete and Rock: Recent Developments*, S.P. Shah, S.E. Swartz and B. Barr (eds.) Elsevier Applied Science, London (1989) 577–586.
10. C.A. Ross and S.T. Kuennen, *Fracture of Concrete and Rock: Recent Developments*, S.P. Shah et al. (eds.), Elsevier, London (1989) 152–161.
11. S. Harsh, Z. Shen and D. Darwin, *American Concrete Institute Materials Journal* 87(5) (1990) 508–516.
12. Z.P. Bažant and R. Gettu, *Fracture of Concrete and Rock: Recent Developments*, S.P. Shah et al. (eds.), Elsevier, London (1989) 549–565.
13. Z.P. Bažant and R. Gettu, *Serviceability and Durability of Construction Materials*, B.A. Suprenant (ed.) (1990) 1113–1123.
14. Z.P. Bažant and R. Gettu, *American Concrete Institute Materials Journal* 89(5) (1992) 456–468.
15. Z.P. Bažant, S.-P. Bai and R. Gettu, *Engineering Fracture Mechanics*, in press.
16. Z.P. Bažant, in *Toughening Mechanisms in Quasi-brittle Materials*, S.P. Shah (ed.), Kluwer Academic Publishers, Dordrecht, (1990) 131–153.
17. Z.P. Bažant, in *Fracture Processes in Concrete, Rock and Ceramics*, J.G.M. van Mier (ed.), Noordwijk, Netherlands (1991).
18. Z.P. Bažant and L. Cedolin, *Stability of Structures: Elastic, Inelastic, Fracture and Damage Theories*, Oxford University Press, New York (1991).
19. Z.P. Bažant and M.T. Kazemi, *International Journal of Fracture* 51 (1991) 121–138.
20. Z.P. Bažant, R. Gettu and M.T. Kazemi, *International Journal of Rock Mechanics, Mining Science & Geomechanical Abstracts* 28(1) (1991) 43–51.
21. Z.P. Bažant and M.T. Kazemi, *International Journal of Fracture* 44 (1990) 111–131.
22. Z.P. Bažant and M.T. Kazemi, *Journal of the American Ceramic Society* 73(7) (1990) 1841–1853.
23. Z.P. Bažant, S. He, M.E. Plesha, R. Gettu and R.E. Rowlands, in *Proceedings International Conference on Dam Fracture*, University of Colorado, V. Saouma et al. (ed.), (1991) 413–425.
24. Z.P. Bažant, *Journal of Engineering Mechanics, ASCE* 110(4) (1984) 518–535.
25. Z.P. Bažant, W.H. Gu and K. Faber, "Effect of change of loading rate on post-peak softening of concrete," Internal report, Northwestern University (1992); also *ACI Materials Journal*, in press.
26. S. He, M.E. Plesha, R.E. Rowlands and Z.P. Bažant, *Dam Engineering* 3 (1992) 139–159.